PPP Without Troposphere Estimation: Impact Assessment of Regional Versus Global Numerical Weather Models and Delay Parametrization

Thalia Nikolaidou, Felipe Nievinski, Kyriakos Balidakis, Harald Schuh, and Marcelo Santos

Abstract

Mapping functions based on global Numerical Weather Models (NWM) have been developed in recent years to model the tropospheric delay in space geodetic techniques such as the Global Navigation Satellite Systems (GNSS). However, the estimation of residual tropospheric delay is still a necessity when high accuracy is required. Additionally, correlation between the estimated tropospheric delay, the receiver clock offset and the station height component, prolongs the time required for the solution to converge and impacts directly the accuracy of the results. In this study, we applied tropospheric corrections from high resolution NWM in GPS processing, in an attempt to acquire rapid and accurate positioning results, waiving the need to estimate residual tropospheric delay. Although high resolution NWM have outperformed standard atmosphere parameters and global models, it is the first time they have been compared against NWM-derived corrections, such as the operational Vienna Mapping Function 1 (VMF1) parameters. The processing strategy employed utilizes different scenarios characterized by their (a) NWM temporal and spatial resolution (b) grid or site-specific domain and (c) delay parametrization. The results were assessed in terms of height components bias, convergence frequency and time as well as residuals of the GPS analysis. Results showed an overall scenarios agreement of about 20 cm for the height component. However, the site-specific domain and high resolution NWM scenarios outperformed the grid-based ones in most of the cases; centimeter compared to decimeter daily height time series bias along faster convergence time constituted their performance. The final height offset with respect to their ITRF14 values was almost three times larger for the grid-based scenarios compared to the site-specific ones. The iono-free least squares adjustment residuals analysis revealed similar patterns for all the scenarios while the estimated heights experienced a reduction on the days of heavy precipitation under most of the scenarios; for some of the stations the advantage of using direct ray-tracing became obvious during those days.

T. Nikolaidou (✉) · M. Santos
Department of Geodesy and Geomatics Engineering, University of New Brunswick, Fredericton, NB, Canada
e-mail: Thalia.Nikolaidou@unb.ca; msantos@unb.ca

F. Nievinski
Department of Geodesy, Federal University of Rio Grande do Sul, Porto Alegre, Brazil
e-mail: felipe.nievinski@ufrgs.br

K. Balidakis
GFZ German Research Centre for Geosciences, Space Geodetic Techniques, Potsdam, Germany
e-mail: balidak@gfz-potsdam.de; schuh@gfz-potsdam.de

H. Schuh
GFZ German Research Centre for Geosciences, Space Geodetic Techniques, Potsdam, Germany

Technische Universität Berlin, Institute of Geodesy and Geoinformation Science, Berlin, Germany
e-mail: schuh@gfz-potsdam.de

International Association of Geodesy Symposia,
https://doi.org/10.1007/1345_2018_44,

Keywords
GPS · High-resolution NWM · Mapping function · Numerical weather model · Precise point positioning · Troposphere modeling · VMF1

Abbreviations

CMC	Canadian Meteorological Centre
ECMWF	European Centre for Medium-Range Weather Forecasts
GAPS	Global Navigation Satellite System Analysis and Positioning Software
GNSS	Global Navigation Satellite Systems
GPS	Global Positioning System
HRDPS	High Resolution Deterministic Prediction System
IERS	International Earth Rotation and Reference Systems Service
IGS	International GNSS Service
MF	Mapping function
NWM	Numerical Weather Model
PP	Point Positioning
PPP	Precise Point Positioning
SD	Slant delay
TUW	Technische Universität Wien
UNB	University of New Brunswick
VMF1	Vienna Mapping Functions 1
ZD	Zenith delay

1 Introduction

In the analysis of Global Navigation Satellite Systems (GNSSS) observations, precise knowledge of the status of the neutral atmosphere (troposphere) is essential. On the one hand, for high-accuracy applications, where estimation of residual zenith tropospheric delay is necessary, existing correlations between the estimated parameters degrade the accuracy of the estimated position, prolong the convergence time and can even lead to faulty parameter estimation when lacking an adequate number of observations. Specifically, correlation between the estimated zenith tropospheric delay, station height and receiver clock offset peaks for observations at high elevation angles (Nilsson et al. 2013) and precise modelling of the troposphere is required to achieve geodetic accuracy. Several methods aiming to decorrelate the estimated parameters and improve the modelling for high-accurate GNSS applications have been developed in past years (e.g., Shi and Gao 2014; Ahn 2016; Yao et al. 2017; Douša et al. 2018). However, the need of supplementary data and/or algorithm adjustment as well as possible shortcomings for real-time applications impede their general implementation.

On the other hand, for navigation or positioning applications where the level of absolute accuracy is not demanding, such as autonomous positioning, i.e., use of single Global Positioning System (GPS) engine or high-rate relative movement tracking, one may omit estimating the tropospheric delay especially when few observations are expected. In such cases, whether single or dual frequency Point Positioning (PP) is utilized, an external input is required for the elimination of the tropospheric delay or as it is commonly called, error. The quality of the external input is critical as any possible error will affect the estimated station height.

Evidently, whether or not the troposphere is estimated, precise modelling of it aids positioning accuracy. Several options exist for the mitigation of the tropospheric error. The most popular of these are "blind" models, which use empirical meteorological parameters or "grid-based" ones, computed via ray-tracing in a Numerical Weather Model (NWM). The parametrization of the tropospheric error at an arbitrary elevation angle, referred to as the slant delay (SD), is performed by means of a mapping function (MF) applied to the zenith delay (ZD) at the site. The current state-of-art and recommended by the latest International Earth Rotation and Reference Systems Service (IERS) conventions MFs (Petit and Luzum 2010), are the Vienna Mapping Functions 1 (VMF1), (Boehm and Schuh 2004) that utilize the European Centre for Medium-Range Weather Forecasts (ECMWF) operational NWM to model the atmosphere.

Although results of such a parametrization can be of sufficient precision, ±3 mm of station height (Böhm 2007) and serve the needs of specific applications, under the presence of atypical atmospheric conditions (e.g., heavy precipitation, severe weather phenomena) the actual meteorological parameters can be far from the model prediction resulting in a computed delay bias that can reach up to 2 m for low elevation angles.

Moreover, when large azimuth asymmetry is present, especially in mountainous or coastal areas, VMF-type MFs are unable to capture the azimuth asymmetry due to their mathematical structure. Existing gradients can reach up to a few decimeters for low elevation angles (Masoumi et al. 2017) introducing a centimeter bias to the height component of the station according to the rule of thumb by Niell and Petrov (2003) and as refined by Boehm and Schuh (2004).

Modelling of such gradients is required (Boehm and Schuh 2013) and an effort was made to generate azimuth dependent MF (Boehm et al. 2005) but its inability to supersede the VMF1 rendered it non-operational (Landskron 2017). Currently, the asymmetric delay component is treated separately by employing linear and nonlinear gradient components (Landskron 2017; Masoumi et al. 2017; Balidakis et al. 2018).

Ray-tracing is able to simulate the delay at each satellite, with or without the need to map the zenith delay. Additionally, the NWM provides the atmospheric 3D information from which one is able to compute or estimate the azimuthal asymmetry.

Recently, NWM with increased spatial and temporal resolution have been made available e.g., by the Canadian Meteorological Centre (CMC), ECMWF and National Center for Environmental Prediction. The scope of this study is to evaluate the improvement in position when 3D ray-tracing (Nievinski and Santos 2010) is utilized, compared to the VMF-parametrization, when alternating the employed NWMs. The presented results demonstrate the impact a GPS Precise Point Positioning analysis (PPP) (Zumberge et al. 1997) when no residual tropospheric delay is estimated.

In the next sections, the research methodology is developed through five adopted scenarios used to retrieve the tropospheric delay. Two scenarios make use of ray-traced delays while the rest use the ZD-MF approach, alternating the employed NWM. More details on the scenarios are provided in Sect. 2. In the sequel, the retrieved delays are employed in PPP and the obtained height position is evaluated against its reference value. The residuals of the PPP analysis are discussed in Sect. 3, and a summary of the outcomes of the study is given in Sect. 4.

2 Data and Methodology

From 6th to 8th June, 2017 a severe precipitation event took place in Victoria Island, BC (Canada), totaling from 24 to 31 mm of rain, depending on the location, the second largest for that month (Fig. 1). Thus, the considered time duration to be examined was chosen from 1st to 10th of June 2017. The research was conducted based on data collected by eight

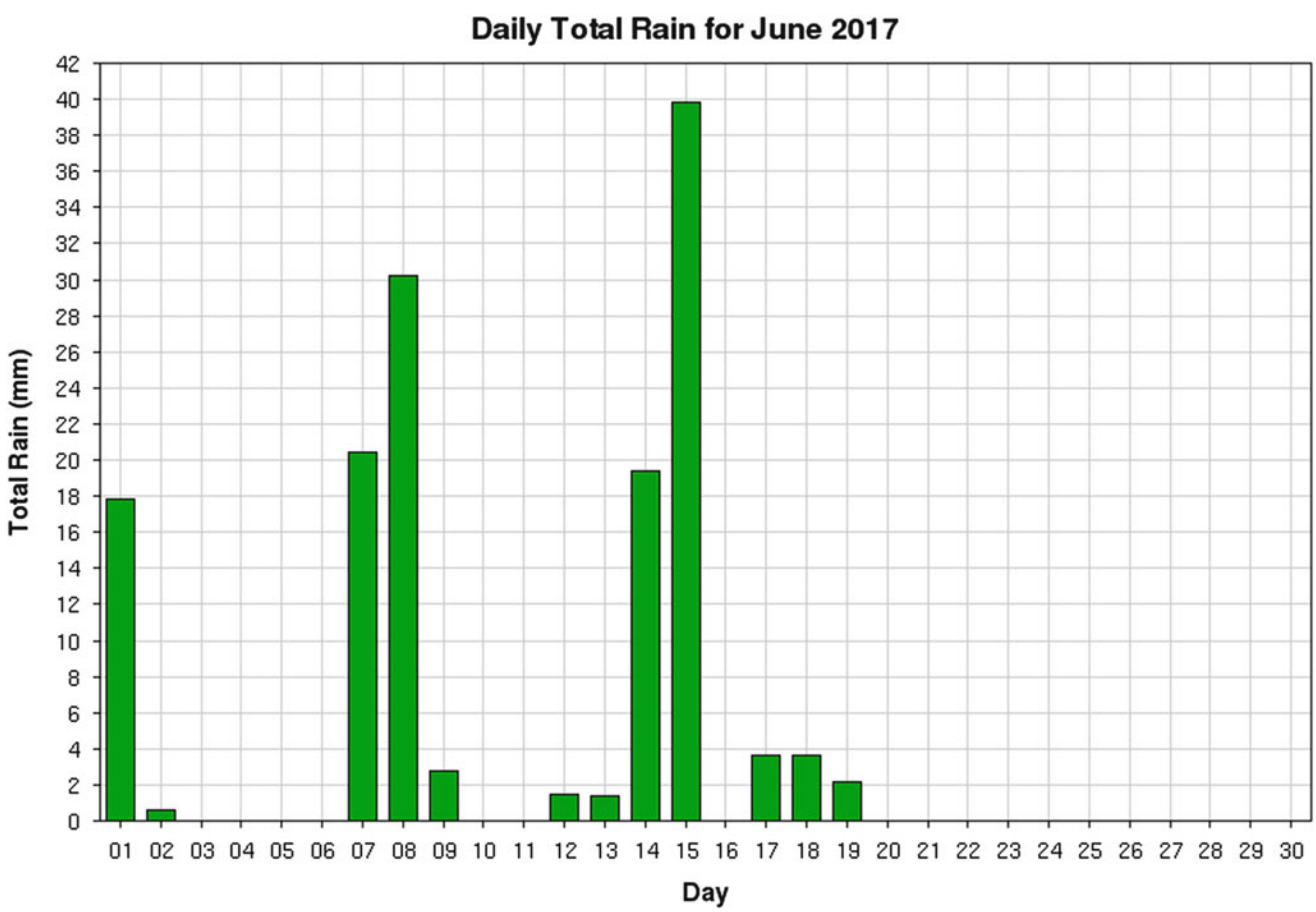

Fig. 1 Total rain records at meteorological station UCLUELET KENNEDY CAMP. Source: Meteorological Service of Canada, Environment and Climate Change Canada

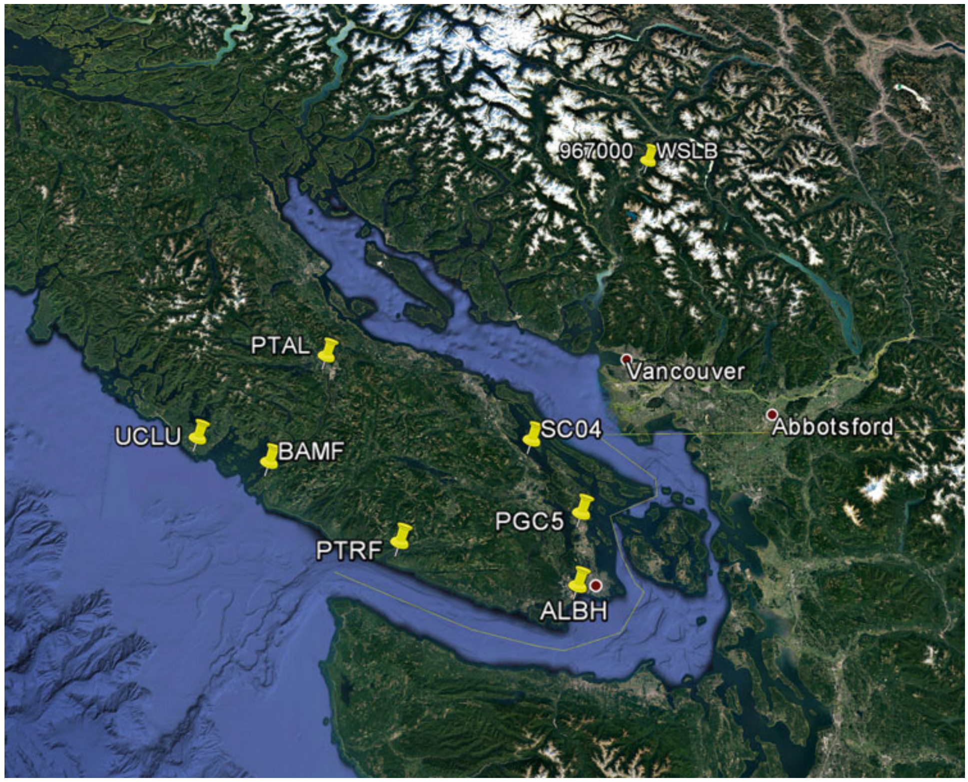

Fig. 2 Location of selected GNSS stations in British Colombia, Canada

GNSS stations (Fig. 2). Seven of those stations are located in the island near the ocean and their proximity allows the study of local meteorological phenomena. The last station, WSLB was chosen for its special location in Whistler, BC, at a height of more than 924 m.

In order to address the scope of this study we define three approaches to retrieve the tropospheric delay and the spatial resolution of the NWM: (a) mapping function along with the zenith delay (ZD-MF) on a geo-grid, (b) ZD-MF specific to each site, (c) direct ray-tracing for all recorded ranges. We also alternated the source used to model the atmosphere: global or regional high resolution (Hi-Res) NWM. In total we had five scenarios: M1, M2, M3, D1 and D2 (Table 1).

Scenario M1 utilizes the VMF1 in the standard way for GNSS analysis i.e., SDs are expressed as the product of the ZDs and MF; the ZD values and MF "a" coefficients are retrieved from the Technische Universität Wien (TUW) on-line repository.[1] The TUW products are interpolated in space (bilinear) and time (cubic) to match the observations' processing interval. We shall call this scenario "*ZD-MF VMF1 – grid*".

Scenario M2 differentiates with respect to M1 only due to the choice of the NWM: M2 uses the Global Deterministic Forecast System (GDPS) from the Canadian Meteorological Center (CMC). Although in a previous study (Nikolaidou et al. 2018) the equality of the products resulted from the ECMWF and CMC NWM has been demonstrated in terms of station position repeatability, under the presence of large azimuthal tropospheric asymmetry, the use of the latter is potentially advantageous due to its increased spatial resolution i.e. CMC has a horizontal resolution of approximately 66 km. Still, the current scenario products were generated at the same resolution as M1's to facilitate the comparison. This scenario is called "*ZD-MF CMC-Glb - grid*".

In scenario M3, although still using the ZD-MF approach, the computation is performed at each site, without grid interpolation, using the High Resolution Deterministic Prediction System (HRDPS), from the CMC. HRDPS has a horizontal resolution of about 2.5 km and a temporal resolution of 1 h. For this scenario, 2D ray-tracing (Nievinski and Santos 2010) – was performed, for the zenith delays and the mapping functions' "a" coefficients, at each site location and at the GPS data interval (5 min). The motivation for the creation of this scenario, is the assessment of the ZD-MF approach with respect to the direct approaches and particularly scenario D2 (explained below). It is referred to as "*ZD-MF CMC-Reg - site*".

Scenario D1 makes use of direct 3D ray-tracing performed for every station-satellite link, at the data interval of 5 min. The CMC GDPS was used to model the atmosphere which has median, with respect to ECMWF and HRDPS, spatial resolution (66 km) and a temporal resolution of 6 h. We shall refer to this scenario as "*SD CMC-Glb - site*".

[1] http://ggosatm.hg.tuwien.ac.at/delay.html.

Table 1 Generated scenarios and their characteristics

Scenario	Approach	NWM	Product spatial resolution	Product temporal resolution	Name
M1	ZD-MF	ECMWF operational	On grid (2 × 2.5°)	Every 6 h	ZD-MF VMF1 – grid
M2	ZD-MF	CMC GLB	On grid (2 × 2.5°)	Every 6 h	ZD-MF CMC-Glb – grid
M3	ZD-MF	CMC HRDPS	At the site	Every 1 h	ZD-MF CMC-Reg – site
D1	SD	CMC GLB	At the site	At observation level	SD CMC-Glb – site
D2	SD	CMC HRDPS	At the site	At observation level	SD CMC-Reg – site

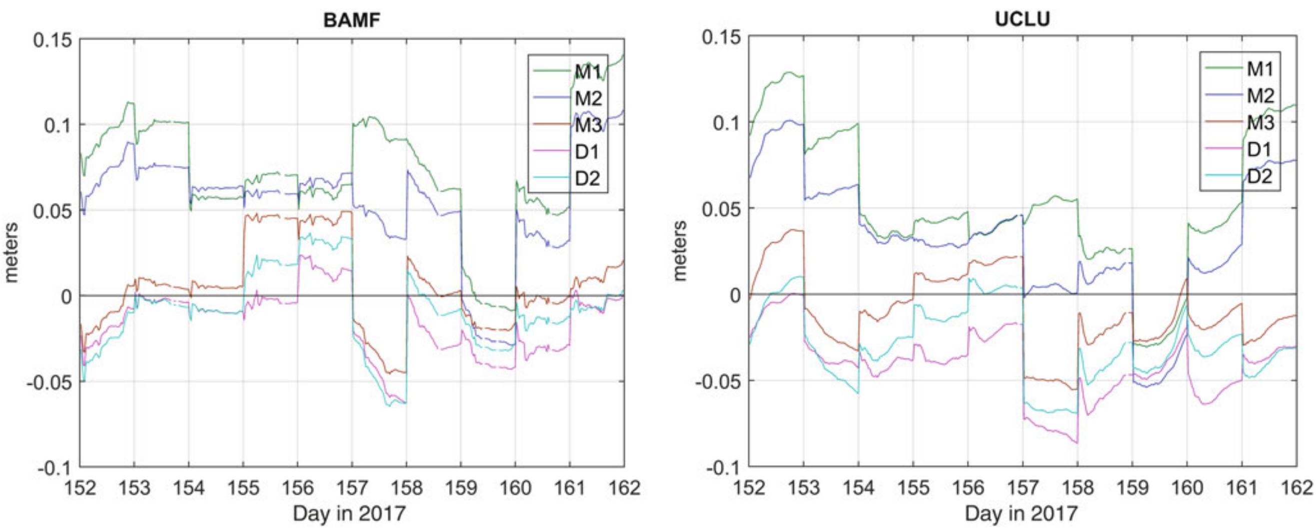

Fig. 3 Height time series (6 h processing) of every scenario: left BAMF and right UCLU station

Finally, scenario D2 represents again direct 3D ray-tracing but using the CMC HRDPS, with its high spatial-temporal resolution. One may suggest this scenario as the most promising one, in matters of predicting accurately the state of the atmosphere and thus the tropospheric delay. We will refer to this scenario as "*SD CMC-Reg - site*".

After acquiring the zenith delays along with the mapping functions and the slant delays for the direction of all recorded ranges, for all the stations and days, each approach was evaluated in GPS Precise Point Positioning (PPP) analysis. The University of New Brunswick's (UNB), available on-line, GNSS Analysis and Positioning Software[2] (GAPS) was employed (Leandro et al. 2007). Precise satellite orbits and clocks were utilized in a GPS-only processing mode and the default options for GAPS processing.[3] Each day was processed individually. It is important to be noted that throughout the analysis no additional tropospheric delay was estimated. In other words, the tropospheric error was left to be mitigated solely by the employed scenario. The results of PPP were analyzed focusing on the height component of each station. To make absolute comparisons, the ITRF14 position of the stations, was considered to be the reference value. For the International GNSS Service (IGS) station ALBH the IGS weekly position was available and thus was used instead. In the following sections, the height bias, the convergence time and the root mean square error of the residuals are examined for each station separately and then the performance for each scenario is summarized.

[2]http://gaps.gge.unb.ca.

[3]http://gaps.gge.unb.ca/strategy.html.

3 Analysis

3.1 Height Time Series Bias, RMSE and 95% Percentile, with Respect to the Reference Value

The scope of this section is to evaluate the height variation within each scenario, with respect to the reference value (ITRF14 or IGS weekly solution), throughout a 6-h worth processing period and for every station. Consequently, each scenario performance is accessed over all stations throughout the processing period of the 10 days.

In the beginning, the estimated height time series, discerned by scenario (choice), were compared with the reference value for all the days and each station. In general, and with the exceptions of few epochs, all scenarios have a maximum disagreement of 20 cm. Although the scenarios seem to

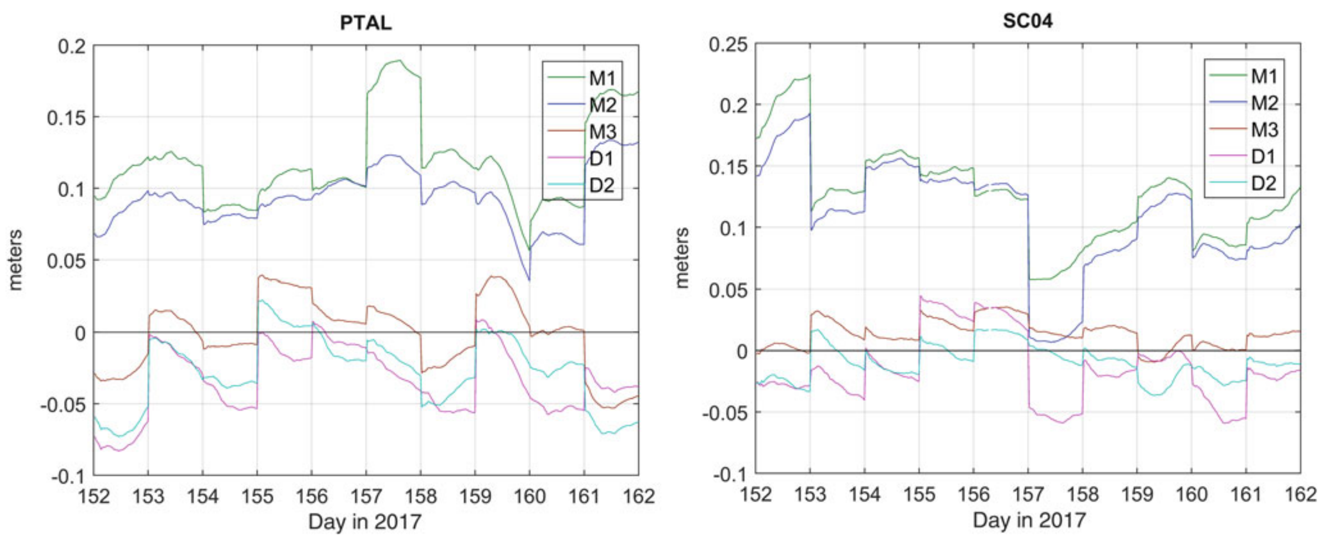

Fig. 4 Height time series (6 h of processing) of every scenario: left PTAL and right SCO4 station

Fig. 5 Height time series bias, averaged over all days, for each scenario and station, when excluding initial convergence time

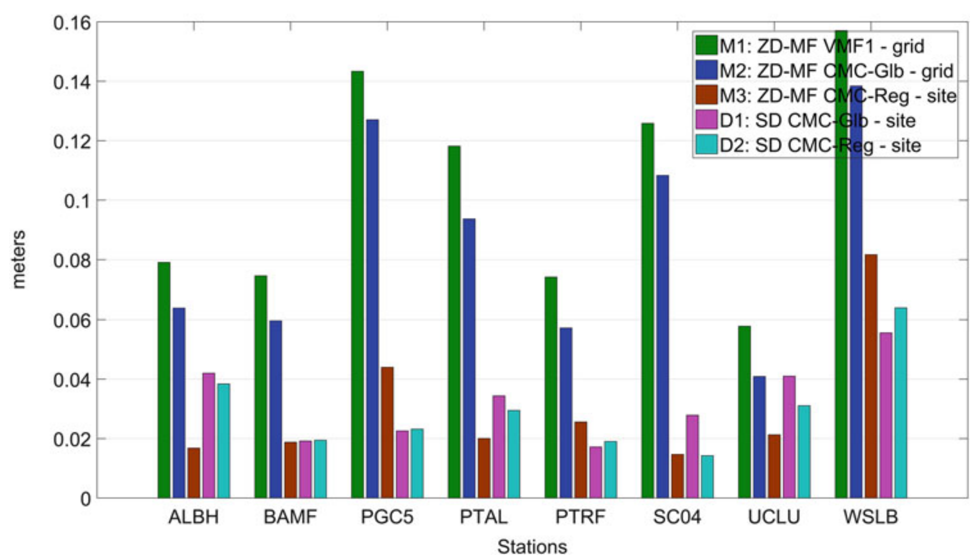

follow each other (Fig. 3),[4] one can easily separate between the grid-based (M1 and M2) and site-specific approaches (Fig. 4). It is noticeable, and further discussed below, that for the latter, the time series bias is smaller. Furthermore, the weather patterns are characteristically portrayed in the figures by the sudden height reduction on the 6th (day of year 157) of June for the stations BAMF, UCLU and SCO4 and then again on the 8th (day of year 159) for all the stations except SC04. These patterns agree well with the total rain records of the nearby meteorological stations.

Examining the total performance of each approach among all stations, although station-based variations exist, the grid scenarios M1 and M2 have overall the largest unsigned biases: 7–19 cm (7–15 cm excluding station WSLB). The (unsigned) biases for M3, D1 and D2 ranging from 4 to 11 cm (4–8 cm excluding WSLB) are the smallest at station PTRF and largest in all scenarios for station WSLB, which is located at an altitude of about 910 m in Whistler. Comparing the grid-based with the site-based scenarios the latter show an improvement ranging from 22% (at UCLU) to 67% (at PGC5) with a mean improvement over all stations of 49%.

Considering that the PPP technique is subject to a convergence time necessary for the parameters to reach their final value, a respective comparison was conducted excluding a mean convergence time of 2 h from every processing (Fig. 5). In this case, the site-based scenarios perform even better with a minimum improvement of 37% (UCLU) and maximum 78% (PGC5). An overall improvement of 65% is achieved. To be noted that at station UCLU, the site-based scenario using the global NWM provides slightly worse or equal, for

[4]An initial window of 2 h, allowed for convergence, has been excluded from the plot.

Table 2 Mean height time series bias for every scenario

Scenario	M1	M2	M3	D1	D2
Bias (m)	0.128	0.110	0.057	0.059	0.057
Bias (m) excl. conv.	0.104	0.086	0.030	0.033	0.030

the two comparisons respectively, results to the grid ZD-MF scenario that uses the same NWM.

The mean unsigned bias (with respect to the reference value) for each scenario is displayed in Table 2. With respect to the whole time series comparison, the grid approaches (M1 and M2) have a mean bias of more than 10 cm while the direct approaches (D1 and D2) and the ZD-MF approach using the Hi-Res NWM (M3) have a mean bias of about 6 cm. On the other hand, excluding convergence period, reduces all the biases by approximately 3 cm, allowing for about 50% improvement for all the site-based scenarios. It is hard to distinguish between the last three scenarios considering the small sample (8 stations) and their millimeter level differences.

The root mean square error (RMSE) of the height time series with respect to the reference value, when considering the full time series, is similar for all approaches and varies only by station; smallest at PTRF and largest at WSLB. Nonetheless, a slightly larger RMSE is noticed for the two grid approaches among all stations with the exception at UCLU. However, excluding the initial convergence period, besides the resulted scale difference, reveals a more spread behavior of each scenario (Fig. 6). Specifically, M1 and M2 have a similar (RMSE) standard deviation (STD), over all stations, of 3.4 cm; M3 has a STD of 2.2 cm followed by D1 and D2 scenarios with 2.3 cm and 1.5 cm respectively. Their respective RMSE mean values are: 11 and 9.2 cm for the M1 and M2 respectively and 3.5 cm on average for all the site-based scenarios (M3, D1 and D2). One may notice the resemblance between the STD and the presumed accuracy of each scenario in view of their parametrization and data source.

Lastly, as another means of assessing the precision of the scenarios employed, the 95% percentile of the height residuals (retrieved height time series – reference value) was calculated for every station and scenario (Fig. 7). As it can be observed, M1 and M2 scenarios have systematically the largest residuals; between the site-based scenarios, none has a systematic behavior over all stations; however, the following can be concluded: for M1 and M2, with a similar behavior, 95% of the residuals are below 18 and 15 cm respectively. This could indicate a slightly smaller frequency of the extreme-outlier retrieved values. The respective number for M3 is 7.7 cm while the two direct ray-tracing scenarios (D1 and D2), have the majority of their residuals below 8.4 cm and 8 cm respectively. Regardless the slightly higher values of the direct scenarios compared to the ZD-MF M3 scenario, which will be discussed later, the results show a potential superiority of the regional NWM handling extreme observations. The mean values of the 95% percentiles are shown in Table 3.

3.2 Convergence to the Reference Value (ITRF14)

Next, the convergence time of each approach was examined. Convergence hereafter is defined with respect to the reference value indicating the confluence of the time series to the latter: the height parameter is considered as "converged" if is within 1 cm deviation from the reference value for at least 20 consecutive minutes. With the above definition for

Fig. 6 Height time series RMSE for each scenario and station, when excluding initial convergence time

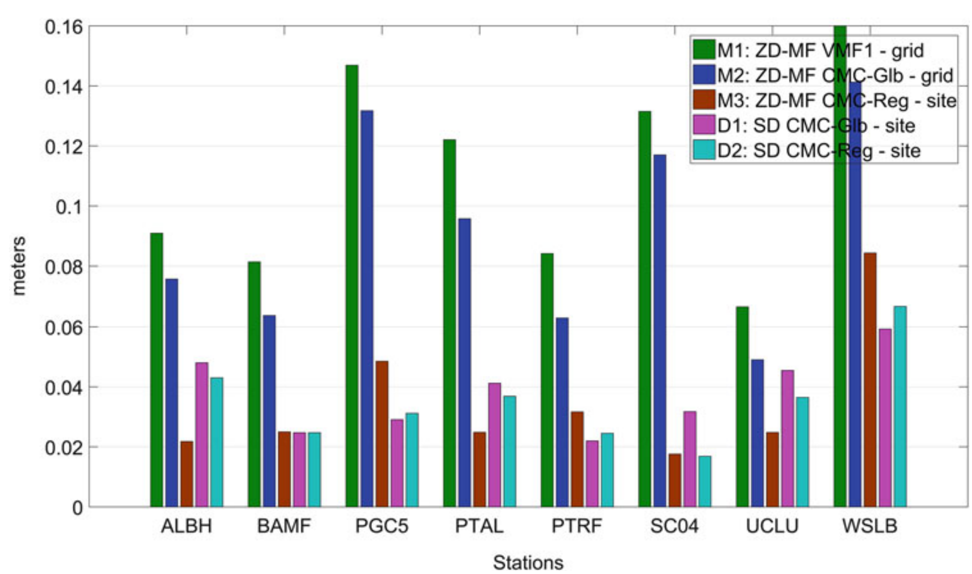

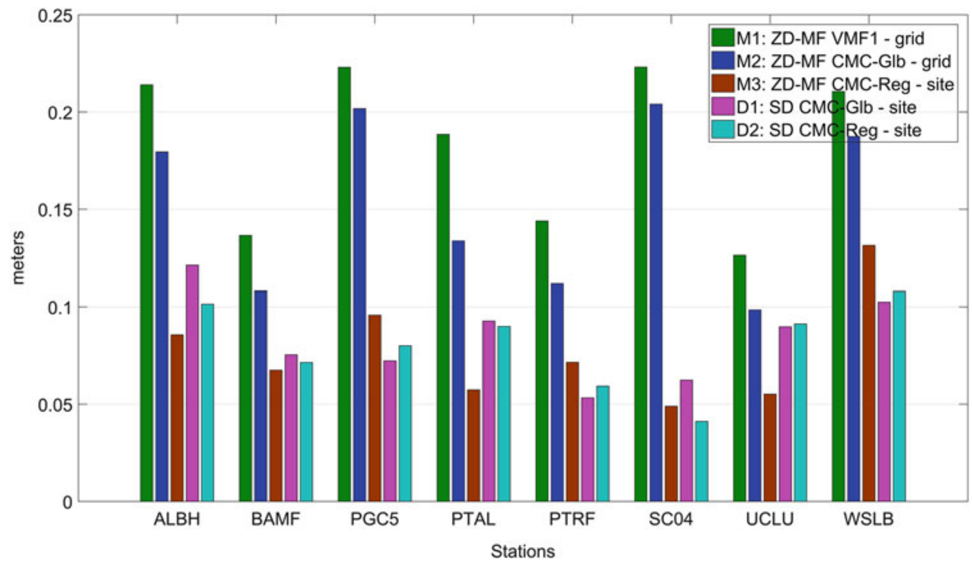

Fig. 7 95% percentile of the height time series residuals for each scenario and station

Table 3 95% percentile of the height time series residuals for each scenario

Scenario	M1	M2	M3	D1	D2
95% percentile (m)	0.183	0.153	0.077	0.084	0.080

convergence, Fig. 8 shows the mean number of times, over the 10 days, an approach has converged for every station. It is noticed that the grid approaches achieve convergence only for half of the stations (M1 and M2 did not converge for stations PGC5, PTAL and WSLB – M1 did not converge also for SC04). The approaches M3, D1 and D2 achieve convergence, at least once, for all stations but WSLB. The meteorological values retrieved from ray-tracing are the result of interpolation in the NWM grid datapoints. Thus, the delay at an arbitrary point (which does not coincide with a NWM datapoint) depicts an average delay of its neighboring NWM datapoints. The inability of the models to reach convergence at WSLB station can be attributed to a poor interpolation due to the ridged topography at the site. In other words, the poor prediction about the slant delay presumably resulted to a biased estimation of the station height.

Considering all the times each approach converged throughout the days and for all stations, M1 and M2, grid approaches, converged only 9% of the times (i.e. 7 times out of all possible 80) (Table 4). The approaches that utilize the Hi-Res NWM (M3 and D2) converged for about half of the times. The approach which utilize the global NWM converged 41% of the times.

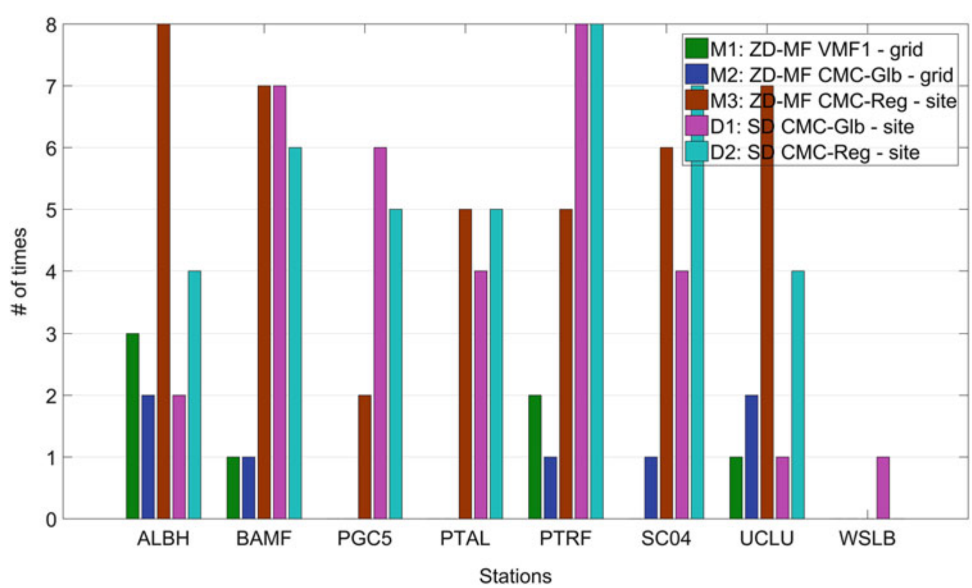

Fig. 8 Mean number of times each scenario converged, to the reference value, for each scenario and station

Table 4 Mean number of times each scenario converged to the reference value for each scenario

Scenario	M1	M2	M3	D1	D2
Total # of times it converged	7	7	40	33	39
% of times it converged	9	9	50	41	49

Table 5 Mean time (in hours) to converge to the reference value for each scenario

Scenario	M1	M2	M3	D1	D2
Mean time (h)	5.33	5.28	3.8	3.95	3.53

3.3 Time Required to Converge to the Reference Value (ITRF14)

Figure 9 shows the mean time taken by each approach to converge to the reference value. It can be seen that for station WSLB all the approaches took longer to converge (except D1 which was longer at UCLU). For station ALBH, in Albert Head, both the grid (M1 and M2) and the D1 and D2 direct approaches required comparable time to converge. The direct approaches showed the best results at station PTRF (again).

Considering all the stations, the direct approach on the Hi-Res NWM (D2) precedes, reaching convergence after about 3.5 h (212 min) followed by the ZD-MF approach (M3) on the same NWM (3.8 h) and the other direct approach on the global NWM (D1) (almost 4 h). About 5.3 h are needed for the VMF1 and UNB-VMF1 approaches (Table 5).

3.4 Final Height Value Bias with Respect to the Reference Value

Continuing the analysis, this section deals with the final value of the height, resulting from 6 h of processing when all estimated parameters are considered to have stabilized and their values attained their maximum precision (in terms of reaching their smallest standard deviation). In Fig. 10, the final height bias with respect to the reference height value is displayed, daily, for every approach and station. Although the height bias differs by day and station among each approach, it is noted that for two stations (BAMF and WSLB) all the approaches are characterized by a positive bias. It can be also seen that for Days Of Year (DOY) 152, 157 and 161 (June 1st, 6th and 10th respectively), three stations (PGC5, PTAL and PTRF) experience unusual lager biases (up to 8 cm) for the grid approaches.

Considering the mean final height bias for every approach per station (Fig. 11), the superior performance of both the direct approaches (D1, D2) is evident as well as the ZD-MF approach but utilizing the Hi-Res NWM at the site (M3). Despite the biases of the grid approaches (M1, M2), which vary based on the station, the UNBVMF1 grid (M2) has consistently smaller mean height bias than M1. The largest height biases in all approaches appear again for station WSLB for the aforementioned reason.

The mean final height bias for each approach is shown in Table 6. The approaches that make use of the Hi-Res NWM have almost equivalent mean final height bias of about 3 cm, with respect to the reference value. The direct approach on the global NWM follows with comparable bias (3.4 cm). As already pointed out the grid approach, that utilizes the CMC-Glb NWM, follows with a mean bias of almost 9 cm whereas the maximum value is at 10 cm for the VMF1 scenario which utilizes the ECMWF's operational model operational NWM.

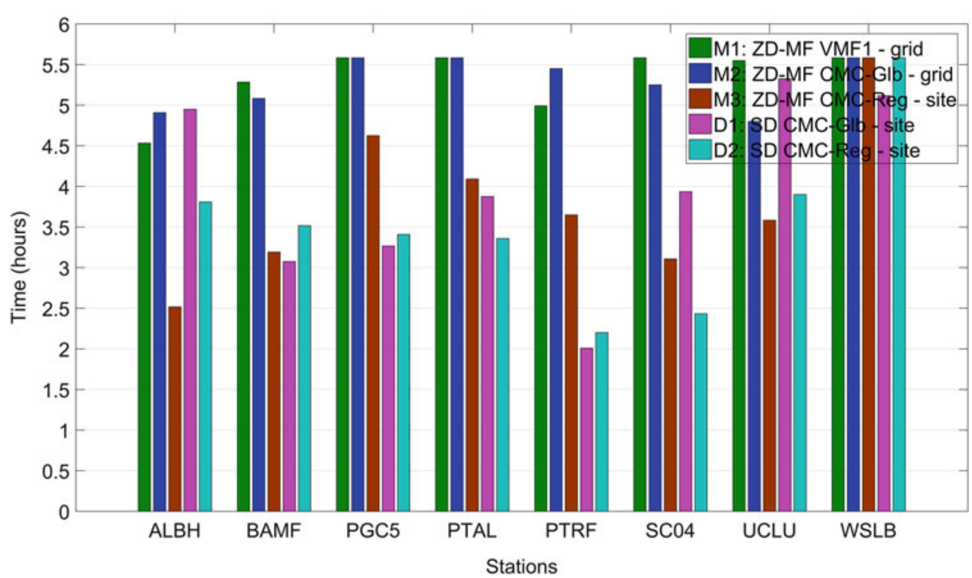

Fig. 9 Mean time (in hours) for each scenario to converge, to the reference value, for each station

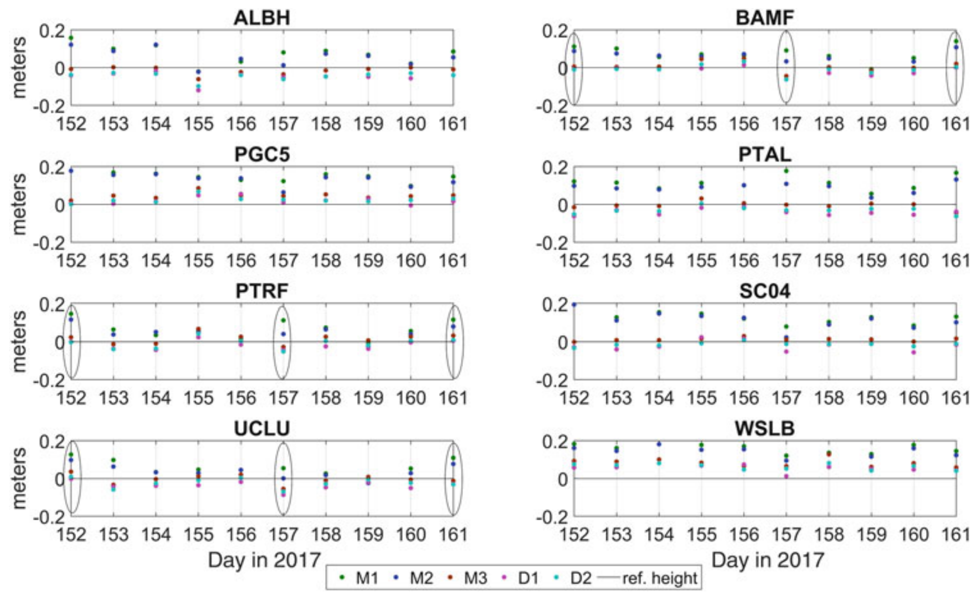

Fig. 10 Final height offset for every scenario, station and day of the study. From top left to bottom right the stations are: ALBH, BAMF, PGC5, PTAL, PTRF, SC04, UCLU and WSLB

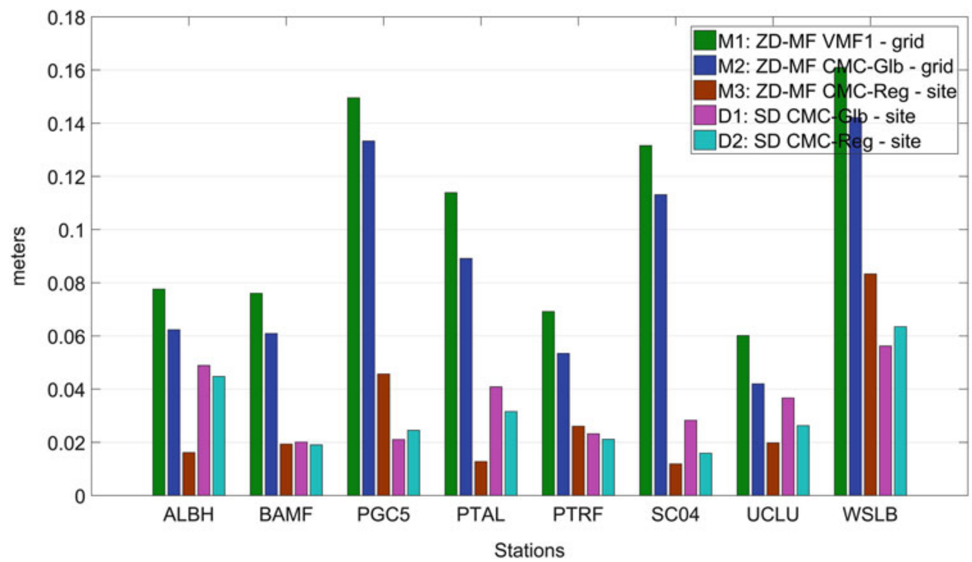

Fig. 11 Mean final height bias for each scenario and station

Table 6 Mean final height bias for each scenario

Scenario	M1	M2	M3	D1	D2
Final bias (cm)	10.9	8.7	2.9	3.4	3.1

Special care should be given to the fact that these results represent a view of the performance of the approaches at the selected sites and it would be ill advised to draw global or even long-term conclusions.

3.5 PPP Analysis Phase Residuals

To complete the analysis, it would be an oversight not to inspect the residuals of the PPP least squares adjustment filter. We examined the phase residuals as the code ones showed only small variations. The RMSE of the phase residuals for every approach and station are displayed in Fig. 12. Contrary to what was expected the direct approaches (D1, D2) have larger mean residuals compared to the ZD-MF approach which uses the Hi-Res NWM (M3); the M3 approach, has consistently the smallest RMSE. In general, the residuals of the direct approaches are comparable with the grid ones.

Table 7 presents the overview for each approach. In spite of the fact that M3 keeps the lead, the RMSE value of the residuals, among the approaches, excluding M3, is 1 cm. Therefore, one may presume that the variations of the residuals are on the noise level and are based on the current conditions, environment and location of the station. Approaches D1 and D2 unexpected large values could be attributed to the proximity of the station to the horizontal

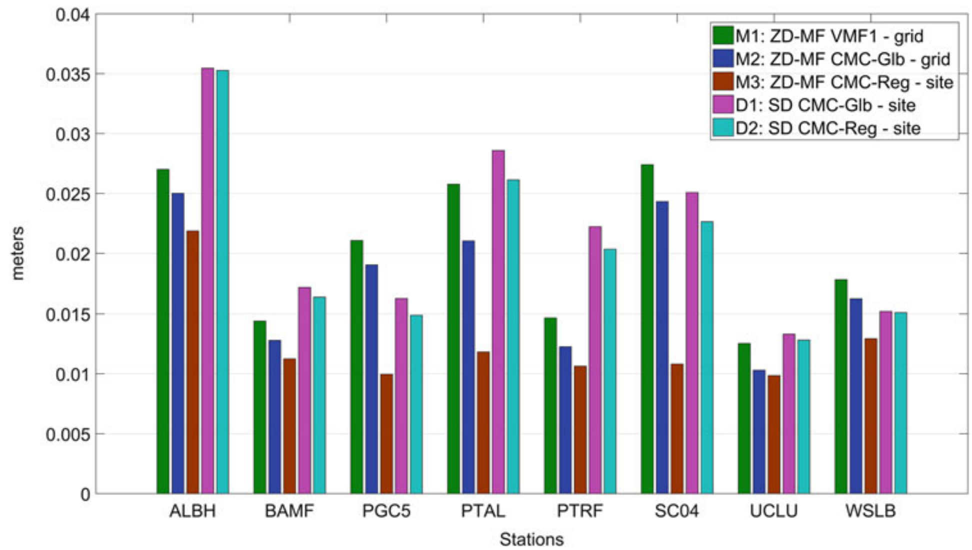

Fig. 12 RMSE phase residuals for each scenario and every station

Table 7 Mean phase residuals for each scenario

Approach	M1	M2	M3	D1	D2
RMSE of phase residuals (m)	0.010	0.009	0.007	0.010	0.010

spatial boundaries of the NWM; for low elevation angles part of the computed delay results outside the NWM limits where a surrogate modeling using climatology is employed. Notwithstanding, it would be considered doubtful to derive conclusions upon the residuals due to their small magnitude which is at the PPP noise level.

4 Conclusion

This study explored two ways of tropospheric delay parametrization in point positioning under using different NWM data sources and parameter resolutions. The delay parametrization using zenith delays and mapping functions was compared against direct ray-tracing at the observation level; three distinct NWM were employed namely the ECMWF, the CMC GLB and HRDPS, and the delay parameters were either interpolated from the nearby grid data points or computed directly at the site. With respect to the NWM employed the case study constitutes the first evaluation of the CMC HRDPS for positioning.

For the zenith delays and mapping functions approach, two grid scenarios using global NWM (ZD-MF VMF1/CMC-Glb) and one site scenario (ZD-MF CMC-Reg) using the regional high-resolution NWM were established, whereas for the direct ray-tracing, two scenarios at the observation level, one for each NWM category: global or regional high resolution, (SD CMC-Glb/Reg) were established.

All the scenarios were evaluated in PPP analysis using the GAPS software, while no tropospheric delay was estimated. Five criteria were used to characterize each scenario's performance: (a) the height time series bias, RMSE and 95% percentile (b) the final height offset, (c) the times each scenario converged, (d) the convergence time itself and (e) the residuals of the ionosphere-free PPP adjustment. In general, all the scenarios agreed within 20 cm, with regard to the height time series bias. However, the grid and non-grid (at the site) approaches could be easily grouped by their cm offset. The mean bias from the reference value was more than 1 decimeter for both grid scenarios and about half for the other ones. Using the site-based scenarios resulted in average 49% improvement in the height time series offset. When excluding an initial convergence period, the improvement rose to 65%. The RMSE of the time series, when considering the full height time series, varied mostly station-wise and was less due to the choice of the scenario. However, excluding the initial convergence period, the average RMSE of the site-based scenarios was 3.5 cm compared to 10 cm of the grid-based scenarios. A 95% percentile analysis of the height residuals showed a potential superiority of the regional NWM compared to the global one when the direct ray-tracing approach was utilized.

With regard to the times each scenario reached the reference value successfully (converged), the ZD-MF CMC-Reg-Site performed the best, achieving convergence for at least 20 consecutive minutes for half of the 10 days of processing. The direct ray-tracing scenarios, SD CMC-Glb-Site/Reg-Site followed closely but both the grid based global ZD-MF ones achieved convergence only 9% of the time. Time-wise, the site scenarios converged about 1.6 h faster compared to the grid ones. The final height offset was about 3 cm for the site scenarios and reached a minimum for the ZD-MF CMC-

Reg-Site. The SD CMC-Glb-Site and Reg-Site scenarios had approximately 10 cm offset from the reference value. Finally, the residuals of all the approaches had a RMSE value of about 10 cm with the exception of the ZD-MF CMC-Reg-Site that had 7 cm. In essence, one may point out that the site scenarios have a clear advantage whether they are employing the ZD-MF or the direct ray-tracing approach. However, the latter has systematically improved results even when compared to the ZD-MF approach at the site, using the same Reg-Site NWM. Lastly, a reduction in the estimated heights was noticed for the heavy precipitation days under most of the scenarios and for some stations the advantage of using direct ray-tracing became obvious.

Acknowledgements The authors would like to thank: the Natural Resources Canada for the GPS data used in this study, belonging to the Canadian Active Control System; the Canadian Meteorological Centre, Environment and Climate Change Canada for providing the data necessary for the creation of the tropospheric parameters and specifically Dr. Edouard Sandrine for her valuable assistance retrieving the data; the Technische Universität Wien (TUW) for providing the VMF1 tropospheric parameters; last but not least, the editor and the two unknown reviewers for their constructive comments and helping to improve the manuscript.

References

Ahn Y-W (2016) De-correlation of tropospheric error and height component on GNSS using combined Zenith-dependent parameter. University of New Brunswick, New Brunswick. http://www2.unb.ca/gge/Pubs/TR306.pdf. Accessed 13 Jul 2018

Balidakis K et al (2018) Estimating integrated water vapor trends from VLBI, GPS, and numerical weather models: sensitivity to tropospheric parameterization. J Geophys Res Atmos 123(12):6356–6372. https://doi.org/10.1029/2017JD028049. Accessed 17 Jul 2018

Boehm J, Schuh H (2004) Vienna mapping functions in VLBI analyses. Geophys Res Lett 31(1):L01603. https://doi.org/10.1029/2003GL018984. Accessed 9 Oct 2017

Boehm J, Ess M, Schuh H (2005) Asymmetric mapping functions for CONT02 from ECMWF. EVGA Work Meet No. 17:64–68

Böhm J (2007) Tropospheric delay modelling at radio wavelengths for space geodetic techniques. 80. https://publik.tuwien.ac.at/files/PubDat_121080.pdf. Accessed 20 Sept 2017

Böhm J, Schuh H (2007) Troposphere gradients from the ECMWF in VLBI analysis. J Geod 81(6):409–421.http://ggosatm.hg.tuwien.ac.at/DELAY/DOC/2007Boehm_etal_LHG.pdf. Accessed 20 Sept 2017

Boehm J, Schuh H (2013) Atmospheric effects in space geodesy. In: Boehm J, Schuh H (eds) Springer atmospheric sciences. Springer, Berlin. https://doi.org/10.1007/978-3-642-36932-2

Douša J et al (2018) A two-stage tropospheric correction model combining data from GNSS and numerical weather model. GPS Solutions 22(3):77. http://link.springer.com/10.1007/s10291-018-0742-x. Accessed 13 Jul 2018

Landskron D (2017) Modeling tropospheric delays for space geodetic techniques. Technischen Universitat Wien, Wien. https://resolver.obvsg.at/urn:nbn:at:at-ubtuw:1-100249

Leandro RF, Santos MC, Langley RB (2007) GAPS: the GPS analysis and positioning software – a brief overview. http://gaps.gge.unb.ca/publications/iongnss2007.leandro.gaps.pdf. Accessed 20 Sept 2017

Masoumi S et al (2017) A directional model of tropospheric horizontal gradients in Global Positioning System and its application for particular weather scenarios. J Geophys Res Atmos 122(8):4401–4425. https://doi.org/10.1002/2016JD026184. Accessed 19 Nov 2017

Niell A, Petrov L (2003) Using a numerical weather model to improve Geodesy. In: Proceedings of 'The State of GPS Vertical Positioning Precision: Separation of Earth Processes by Space Geodesy' meeting held in April 2003 in Luxemburg. http://arXiv.org/physics/0401118

Nievinski FG, Santos MC (2010) Ray-tracing options to mitigate the neutral atmosphere delay in GPS. Geomatica 64(2):191–207

Nikolaidou T et al (2018) Impact of different NWM-derived mapping functions on VLBI and GPS analysis introduction and background. Earth Planets Space 70:95. https://doi.org/10.1186/s40623-018-0865-x. Accessed 18 Jul 2018

Nilsson T et al (2013) Path delays in the neutral atmosphere. Springer, Berlin, pp 73–136. https://doi.org/10.1007/978-3-642-36932-2_3. Accessed 22 Sept 2017

Petit G, Luzum B (2010) International Earth rotation and reference systems service (IERS) service international de la rotation terrestre et desSys emes de Référence IERS conventions (2010), Frankfurt am Main. https://www.iers.org/SharedDocs/Publikationen/EN/IERS/Publications/tn/TechnNote36/tn36.pdf;jsessionid=835D089F780AD79FEC5C1A69FD434DB5.live2?__blob=publicationFile&v=1. Accessed 6 Feb 2018

Shi J, Gao Y (2014) A troposphere constraint method to improve PPP ambiguity-resolved height solution. J Navig 67:249–262

Yao Y et al (2017) Enhancing real-time precise point positioning with zenith troposphere delay products and the determination of corresponding tropospheric stochastic models. Geophys J Int 208(2):1217–1230. https://academic.oup.com/gji/article-lookup/doi/10.1093/gji/ggw451. Accessed 20 Mar 2017

Zumberge JF, Heflin MB, Jefferson DC et al (1997) Precise point positioning for the efficient and robust analysis of GPS data from large networks. J Geophys Res Solid Earth 102:5005–5017. https://doi.org/10.1029/96JB03860